Chinese Journal of Aeronautics, 2013,26(3): 594–600

Chinese Society of Aeronautics and Astronautics
& Beihang University

Chinese Journal of Aeronautics

cja@buaa.edu.cn
www.sciencedirect.com

Infrared radiation signature of exhaust plume from solid propellants with different energy characteristics

Wang Weichen [a], Li Shipeng [b,*], Zhang Qiao [a], Wang Ningfei [b]

[a] *China Academy of Space Technology, Beijing 100094, China*
[b] *School of Aerospace Engineering, Beijing Institute of Technology, Beijing 100081, China*

Received 16 March 2012; revised 22 July 2012; accepted 15 October 2012
Available online 17 May 2013

KEYWORDS

Coupled solution;
Energy characteristics;
Exhaust plume;
Infrared radiation signature;
Solid propellant

Abstract The infrared radiation signature of the plume from solid propellants with different energy characteristics is not the same. Three kinds of double-base propellants of different energy characteristics are chosen to measure the infrared spectral radiance from 1000 cm^{-1} to 4500 cm^{-1} of their plumes. The radiative spectrum is obtained in the tests. The experimental results indicate that the infrared radiation of the plume is determined by the energy characteristics of the propellant. The radiative transfer calculation models of the exhaust plume for the solid propellants are established. By including the chemical reaction source term and the radiation source term into the energy equation, the plume field and the radiative transfer are solved in a coupled way. The calculated results are consistent with the experimental data, so the reliability of the models is confirmed. The temperature distribution and the extent of the afterburning of the plume are distinct for the propellants of different energy characteristics, therefore the plume radiation varies for different propellants. The temperature of the fluid cell in the plume will increase or decrease to some extent by the influence of the radiation term.

1. Introduction

Infrared radiation signature of a rocket motor exhaust plume is the most noticeable characteristic of flight vehicles. Research on the radiation mechanism of exhaust plumes is important for the design of underbody components and detection systems in the aircraft, the stealth performance, and improvement of ingredients of the solid propellants. Fuel rich gas is generated during the combustion process of the propellants in the solid rocket motor. After it is injected into the air, some oxygen is entrained into the plume and then the afterburning reaction occurs in the mixing layer of the plume. Afterburning can greatly increase the temperature and the radiation intensity of the plume near field.[1]

The radiative transfer calculation in the plume involves many complicated factors, such as combustion calculations for the propellants, plume field calculations and radiative transfer calculations; therefore valid experimental data are helpful for improving the calculation codes. Harwell et al.[2] used an infrared radiation detector to measure the radiation intensity of the plume field. Deimling et al.[3] used a spectrometer to measure the infrared radiation spectral characteristics from 1.2 μm to 14 μm of three different types of solid propellants. Devir et al.[4] used Fourier transfer infrared spectrometer

* Corresponding author. Tel.: +86 10 68918107.
E-mail address: lsp@bit.edu.cn (S. Li).

Peer review under responsibility of Editorial Committee of CJA.

ELSEVIER Production and hosting by Elsevier

1000-9361 © 2013 Production and hosting by Elsevier Ltd. on behalf of CSAA & BUAA. Open access under CC BY-NC-ND license.
http://dx.doi.org/10.1016/j.cja.2013.04.019

(FTIR) and forward-looking infrared spectrometer (FLIR) to measure the infrared radiation intensity from 1.5 μm to 5.5 μm and the infrared radiation images for a small solid rocket motor.

The coupled solution of flow field and radiative transfer can significantly increase the resolution of radiation calculations, while they were generally solved independently in previous studies. SIRRM (Standardized Infrared Radiation Model) is one of the widely used codes for radiative transfer calculations in plumes, which is based on the heat flux method. Nelson[5,6] used SIRRM[7,8] code to calculate the infrared radiation signature in various conditions for a typical motor including the base heating effect of the plume. Surzhikov[9–11] made full discussions on the critical factors and different models in the radiative calculations of the plume using the Monte Carlo method. Burt and Boyd[12,13] simulated gas-particle multiphase flow of a plume in a vacuum using the direct Monte Carlo method. Liu et al.[14] developed the code GRASP for radiation transfer calculations in exhaust plume using the discrete ordinates method. However, the radiative transfer calculation methods discussed above are based on results of plume field calculations, which means that the radiative transfer calculations and the plume field calculations are carried out independently.

Three kinds of double-base solid propellants of different energy characteristics were selected in our work, and the infrared spectral radiance from 1000 cm^{-1} to 4500 cm^{-1} of their plumes was measured. The radiative spectrum and the infrared images in the 4.3 μm band were obtained in the tests. The radiative transfer calculation models for the exhaust plume from the solid propellants were established. By including the radiation source term in the energy balance equation, the plume field calculation and the radiative transfer calculation were carried out in a coupled way. The discrete ordinates method was used to solve the radiative transfer equation. The distribution of the radiative illumination in typical bands and radiative illumination contours were obtained.

2. Radiative experiment

2.1. Test principal

Three kinds of double-base propellants of different energy characteristics were chosen, and the FTIR was used to measure the infrared radiation signature of the plume. The infrared detectors of the FTIR were InSb and MCT, the spectral range was from 1000 cm^{-1} to 4500 cm^{-1}, the spectral resolution was 4 cm^{-1}, and the scan frequency was 8 Hz. A fibercable was used to connect the FTIR and the computers. Liquid nitrogen was used to cool the infrared detectors. The error bar within the experiments is 5%.

Fig. 1 shows the placement of the infrared detecting instrument for the test. The FTIR was 4.3 m away from the axis line of the plume, and the test object was a circular optical spot located in the axis line of the plume, whose diameter was 60 mm. The spot was 0.5 m away from the exit plane of the nozzle. The FTIR detects the infrared energy emitted from the test spot, and outputs the spectral radiance I_λ ($W/(cm^2 \cdot str \cdot cm^{-1})$) of the test spot.

2.2. Propellant formulations

Three kinds of double-base propellants of different energy characteristics were chosen, and the infrared radiation signature of their plumes was measured. Table 1 shows the formulations of the three propellants.

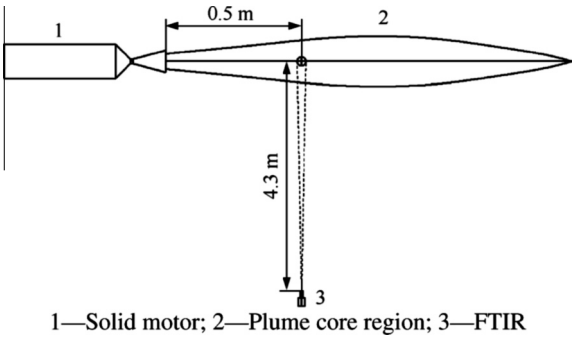

Fig. 1 Placement of measurement equipment.

2.3. Data analysis method

In engineering applications of infrared detecting systems, the infrared detectors are usually designed to measure infrared energy emitted from the objects in discrete bands, therefore it is important to study the distribution of the infrared energy in the typical band. The primary species in the plume are CO_2, H_2O and CO and because of their spectral characteristics, there are specific radiation peaks across the spectrum (from 1000 cm^{-1} to 4500 cm^{-1}). To study the infrared radiation in some band, the spectral range can be divided into seven parts. The detailed division is shown in Table 2. The spectral radiance I_λ ($W/(cm^2 \cdot str \cdot cm^{-1})$) is integrated in every band, and then the radiation intensity I($W/(cm^2 \cdot str)$) in the detecting direction of the FTIR of each band is determined. The radiative illumination E (W/m^2) of the test spot can be obtained by the integration of the radiation intensity in solid angles (zenith angle θ and zimuth angle φ) of the hemisphere. The integral equation of E is shown as follows:

Table 1 Formulations of test propellants.

Ingredients	dbp-1 (%)	dbp-2 (%)	dbp-3 (%)
Nitrocellulose (NC)	56.0	47.3	20.5
Nitroglycerine (NG)	34.7	33.6	27.7
Octogen (HMX)	0	9.1	41.0
Else	9.3	10.0	10.8

Table 2 FTIR spectral band divisions.

No.	Start wave number (cm^{-1})	Endwave number (cm^{-1})	Wavelength (μm)
1	1000	1600	8.12
2	1600	1950	5.69
3	1950	2150	4.30
4	2150	2400	8.82
5	2400	3100	3.70
6	3100	3800	2.70
7	3800	4500	2.40

$$E = \int_{\phi=0}^{2\pi} \int_{\theta=0}^{\pi/2} I \cos\theta \sin\theta \mathrm{d}\theta \mathrm{d}\phi \quad (1)$$

3. Physical models and calculation methods

3.1. Physical models

The heat released from the combustion reaction has a great effect on the flow field; it can increase the temperature of flow field as well as enhance the infrared radiation in the plume near field. The combustion reaction is considered in the flow field calculation by introducing the reaction source term into the energy equation of the flow field. The flow field and the radiation heat transfer can be calculated in a coupled way by introducing the radiation source term into energy equation of the flow field. The energy equation of the flow field is written as

$$\frac{\partial}{\partial t}(\rho E_q) + \nabla(\boldsymbol{v}(\rho E_q + p)) = S_c + S_r + \nabla \cdot (k_{eff} \nabla T - \sum_j h_j \boldsymbol{J}_j + (\tau_{eff} \cdot \boldsymbol{v})) \quad (2)$$

where $E_q = h - p/\rho + \boldsymbol{v}^2/2$, p is the pressure, ρ is the density, $\boldsymbol{v}$ is the velocity, $h = \int_{T_{ref}}^{T} c_p \mathrm{d}T$, c_p is the constant pressure specific heat, $T_{ref} = 298.15$ K; S_c is the reaction source term, representing the heat of chemical reaction; S_r is the radiation source term, representing the heat of emission and transfer process, which can be obtained by solving the radiation transfer equation; $k_{eff} = (k + c_p \mu_t/Pr)$, k is the thermal conductivity, P_r is Prandtl number, μ_t is the turbulence viscosity coefficient; τ_{eff} is the deviator stress tensor. The last three terms on the right-hand side of equation represent energy transfer due to conduction, species diffusion, and viscous dissipation, respectively.

The combustion reaction mainly occurs in the plume near field. In this region the flow is supersonic, and the Arrhenius law[15] can be used to describe the detailed chemical mechanism in the afterburning plume. The main reactions in afterburning are H_2/CO oxidization reactions, therefore H_2/CO oxidization system[16–19] was used to simulate the afterburning phenomenon. The reaction mechanisms used are listed in Table 3.

The finite volume method was used to solve the control equations of the flow field. RNG k-ε model[18] was used to simulate the turbulence flow. The near wall boundary condition adopted a standard wall function. The discrete ordinates method was used to solve the radiation transfer equation, and the stiff chemistry solver was used to increase the stability of the reaction calculation.

Table 3 Chemistry reaction model in the plume.

$CO + O + M = CO_2 + M$
$CO + OH = CO_2 + H$
$H_2 + OH = H_2O + H$
$H_2 + O = OH + H$
$H + O_2 = OH + O$
$OH + OH = H_2O + O$
$H + H + M = H_2 + M$
$O + O + M = O_2 + M$
$O + H + M = OH + M$
$H + OH + M = H_2O + M$

3.2. Plume field calculation

The axial two-dimensional calculation domain was used to solve the plume flow field and radiation transfer process. The length and height of the plume calculation region are 10 m and 1 m respectively. The diameter of the chamber is 50 mm, and the nozzle contraction angle is 45°, and the nozzle expansion ratio is 2.3. A schematic of the computation region is shown in Fig. 2. The computational mesh around the nozzle exit is shown in Fig. 3.

The inlet boundary type of the nozzle is pressure inlet, and chamber pressure is 7 MPa. The outlet boundary type of the plume is pressure far field, and the atmosphere pressure is 101325 Pa with the atmosphere temperature of 300 K. External radiation heat sources are neglected. The minimum free energy method was used to carry out the thermodynamic calculation for the three propellants, and the calculated mass fractions of main gas species in the chamber are shown in Table 4. The temperatures of the gaseous combustion products of the propellants are 2151 K, 2646 K and 3291 K, which shows that there are obvious differences in the energy characteristics of the propellants. From the formulations of the propellants shown in Table 1, the changes of the content of the energetic

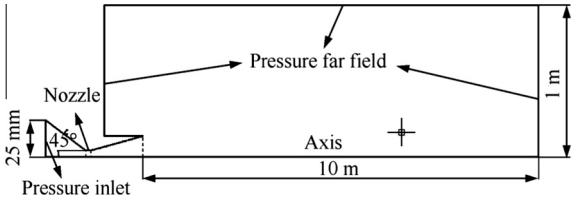

Fig. 2 Schematic of computation region.

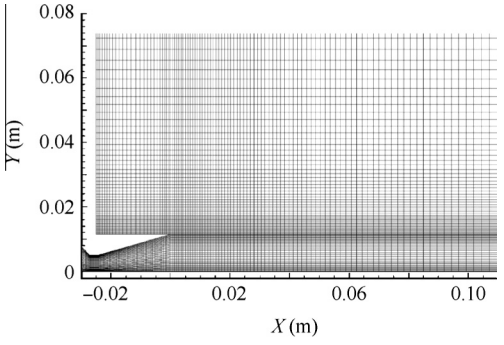

Fig. 3 Mesh around nozzle exit.

Table 4 Calculated gaseous product species mass fractions.

Species	dbp-1	dbp-2	dbp-3
H_2O	0.1004	0.1172	0.1792
CO_2	0.3817	0.3614	0.3411
CO	0.3541	0.3366	0.2136
H_2	0.0163	0.0142	0.0057
O_2	0	0	0
N_2	0.1475	0.1705	0.2604

ingredients such as NG and HMX may be the main cause of the differences in the energy characteristics of the propellants.

3.3. Radiation calculation

Radiation calculations were coupled with the flow field calculations. Since the radiation transfer is directional, the transfer direction in elemental volume is discretized by zenith angle θ and azimuth angle φ. The discrete ordinates method[20] of second order upwind scheme was used to solve the radiation transfer equation in every transfer direction.

The radiative participating media is gas, whose scattering effect is very small and can be ignored. The numerical average method was used to calculate the absorption coefficients based on the molecular spectroscopic database HITRAN 2004.[21,22]

To study the infrared radiation signature in the seven spectral bands, the flow field and radiation transfer were calculated in every spectral band.

4. Results and discussions

4.1. Plume characteristics

Fig. 4 shows the temperature contours of the plume of three propellants. As seen in the figures, the length and the width of the high temperature region in the plume of dbp-1 propellant are relatively small. The temperature of the middle and rear part of the plume core region of dbp-2 and dbp-3 propellants are comparatively high. This is because fuel rich species in the combustion gas mix and react with the oxygen in the air in this region. The afterburning reactions in the plume of dbp-3 propellant occur relatively closer to the exit of the nozzle.

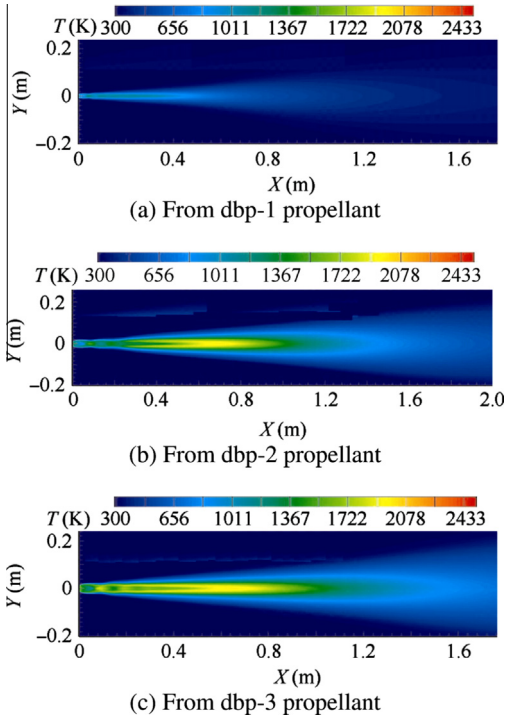

Fig. 4 Temperature contours of the plume from three propellants.

Fig. 5 shows the temperature distributions in the axis line of the frozen plume and the afterburning plume for the propellants. As seen in the figure, the temperature along the plume up to 0.4 m fluctuates with the flow structure of the Mach wave systems. There is a temperature peak at 0.7 m in the axis line of the plume for the dbp-2 and dbp-3 propellants, which is caused by the afterburning reactions. The temperature peaks caused by the afterburning of dbp-2 and dbp-3 propellants are close to each other. The afterburning reactions increase the temperature of the core plume (from 0.4 m to 0.8 m) of dbp-2 and dbp-3, making the flow structure of their plumes similar to each other. So, when the gas moves forward along the axis, their temperature traces become the same after 0.85 m. However, there is no such a temperature peak in the same position of the plume of dbp-1 propellant, which indicates that there are no obvious afterburning reactions. The reason is that the gas temperature of dbp-1 in chamber is much lower than the other two, and the temperature of dbp-1 plume is so low that the afterburning reactions are not activated in the axis of the plume.

The comparison of temperature in the axis line between the afterburning plume and the frozen plume is shown in Fig. 5. It can be seen that the temperature increase of the afterburning plume from dbp-2 propellant is most pronounced, while there is no temperature increase along the plume axis for dbp-1 propellant, which means that the afterburning phenomenon is very weak in this region.

The main chemical species in the plume are H_2O, CO_2, H_2 and CO, among which H_2O and CO_2 are stronger infrared emitters. Figs. 6 and 7 illustrate the mass fraction contours of the four species above in the plume from dbp-3 propellant. As seen in the figure, the mass fraction of the four species changes with the flow structure of Mach wave systems. In

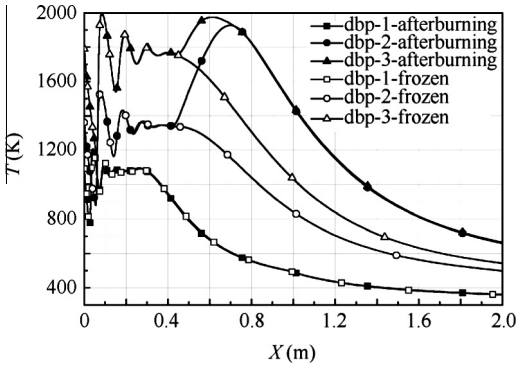

Fig. 5 Temperature distributions in axis line of frozen plume and afterburning plume from three kinds of propellants.

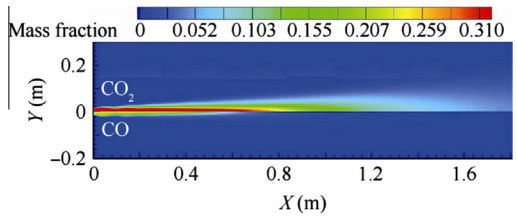

Fig. 6 Mass fraction contour of CO_2 and CO in the plume from dbp-3 propellant.

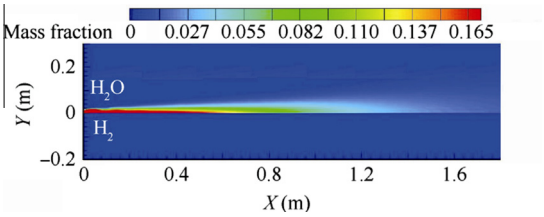

Fig. 7 Mass fraction contour of H_2O and H_2 in the plume from dbp-3 propellant.

the mixing layer, the concentrations of H_2O and CO_2 increase, while the concentrations of H_2 and CO decline, which is caused by afterburning reactions in the plume.

4.2. Infrared signature

Fig. 8 shows the distribution of the radiative illumination in the seven spectral bands at the monitor point in the plume for the propellants. As seen in the figure, the radiative illumination in band 4 is the greatest for all the propellants, which is mainly caused by the infrared emissions of CO_2 and CO. As for band 1, the radiative illumination is also significant, which may be caused by the long wavelength emission of H_2O. The experimental results show that the radiative illumination in band 7 is relatively weak, because the main radiative species are H_2O and CO, whose infrared radiation in this band is fairly small. The radiative illumination in band 5 is minimal, because there is no species specific emission in this band. There are significant differences in the infrared radiation power of the plume from the three propellants, and the infrared radiative illumination of plume from dbp-1 propellant is rather weak in all bands. The difference of the energy characteristic of the propellant may be the main reason for the variation. As seen in the figure, the calculation results can reflect the trend of the infrared radiation in every band, and the deviations from the experimental data are reasonable.

Fig. 9 shows the radiative illumination contours in band 4 of the plume from three propellants. As seen in the figures, the change of the radiative illumination is consistent with the change of the temperature of the plume, and the radiative illumination is relatively higher in the middle and rear part of the plume. This is because the afterburning reactions in these regions are sufficient enough that the temperature of the flow field is relatively higher, and consequently, the infrared radiation of the gas is stronger. In the axial direction of the plume, radiative illumination is relatively higher, and the infrared energy can radiate further. In the vertical direction, the radiative illumination declines rapidly. The distribution of the radiative illumination reflects the energy characteristics of the propellants. The area of high temperature is larger in the infrared image of dbp-3 propellant than others, while there is nearly no high temperature area in the infrared image of dbp-1 propellant, which is because the energy level of dbp-1 propellant is quite low.

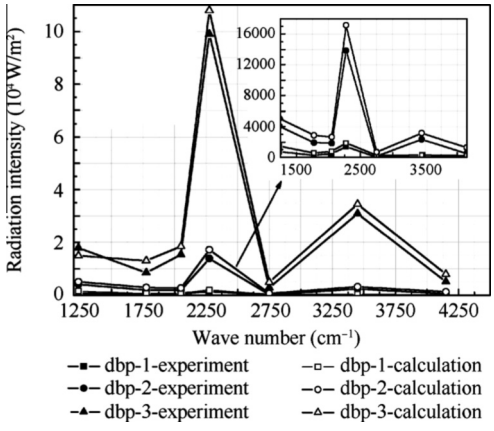

Fig. 8 Distribution of radiative illumination in every typical spectral band at the monitor point in the plume from the three propellants.

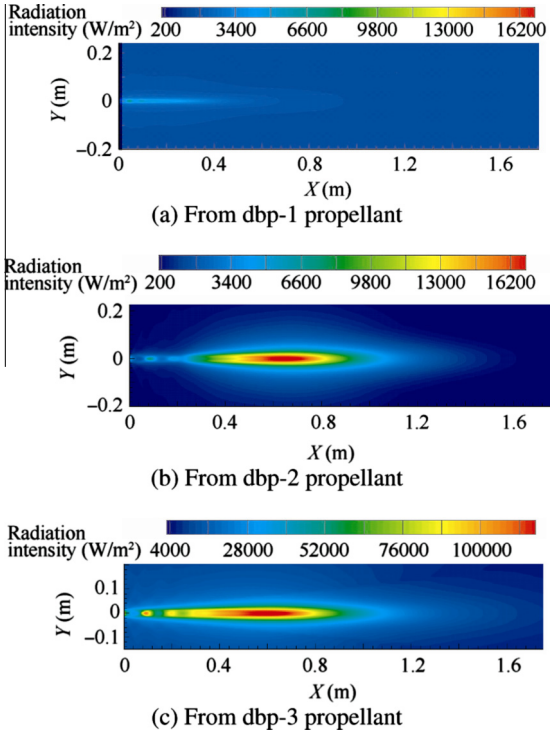

Fig. 9 Radiative illumination contours in band 4 of the plume from three propellants.

Fig. 10 shows the distribution of the radiative illumination in the axis line of the plume of the three propellants. As seen in the figure, the radiative illumination up to 0.4 m fluctuates with the temperature of the flow field. There is a peak of the radiative illumination at 0.65 m in the axis line of the plume of dbp-2 and dbp-3 propellants. There are obvious differences in the radiative illumination between the propellants, because the energy characteristics of each propellant are different.

Fig. 11 shows the influence of the radiation source term on the temperature distribution in the axis line of the plume for the propellants. The temperature distributions in the axis line of the plume with (coupled solution) and without (decoupled solution) the radiation source term are compared. As seen in the figure, the temperature distribution in the axis line of the plume is nearly identical for the coupled and decoupled solutions for dbp-1 propellant. The temperature peak moves a little forward with the coupled solution for dbp-2 propellant, the temperature before 0.7 m with the coupled solution is relatively higher than that of the decoupled solution, and the tempera-

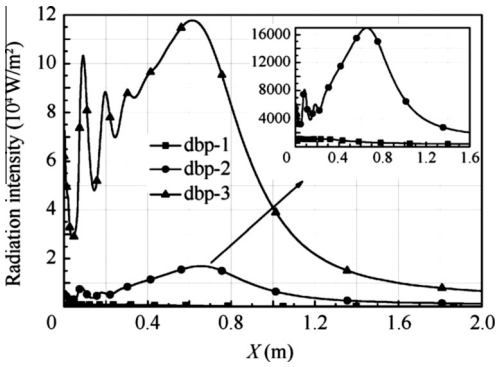

Fig. 10 Distribution of radiative illumination in axis line of the plume of the three propellants.

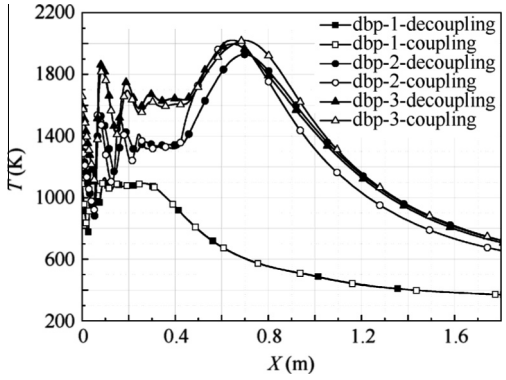

Fig. 11 Influence of radiation source term on the temperature distribution in axis line of the plume from the three propellants.

ture after 0.7 m with the coupled solution is relatively lower than that of the decoupled solution. For dbp-3 propellant, the temperature before 0.7 m with the coupled solution is slightly lower than that of the decoupled solution, and the temperature after 0.7 m with the coupled solution is relatively higher than that of the decoupled solution, and the variation amplitude of the temperature in the axis line of dbp-3 propellant is smaller than that of dbp-2 propellant. From the viewpoint of energy conservation, when the radiation energy emitted out of the cell is larger than the received radiation energy from the circumambient cells, the temperature of the cell will decrease with coupled solution. For the decoupled solution, the temperature of the cell will increase. The results indicate that it is necessary to adopt the coupled solution to calculate the flow field and the radiative transfer simultaneously.

Fig. 12 shows the influence of the radiation source term on the temperature distribution in the plume near field for dbp-2 propellant. As seen in the figure, when the radiation source term is included, the temperatures in the mixing layer and around the axis line of the plume increase to some extent, while the temperatures in the rear part and the peripheral part of the plume decrease. The temperatures in the mixing layer and around the axis line of the plume are very high, and the radiation power is quite strong. When the radiation source term was included in the coupled solution, the radiative heating of the high temperature region is significant; consequently the

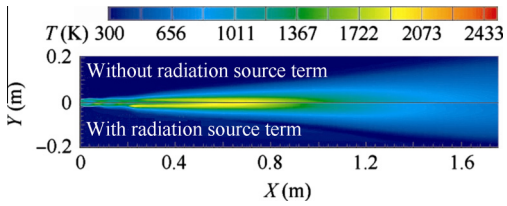

Fig. 12 Influence of radiation source term on temperature distribution in the plume near field from dbp-2 propellant.

temperature of the fluid will increase. While in the rear part and the peripheral part of the plume, the emitted radiation energy and the dissipation radiation energy are larger than the radiation energy received from the surrounding fluid cells, therefore the temperature will decrease. This trend agrees with the energy conservation principle. Based on the above studies, it can be concluded that the included radiation source term will change the temperature of the plume field to some extent, and it is necessary to apply the coupled solution for the plume calculation.

5. Conclusions

(1) Three kinds of double-base solid propellants of different energy characteristics were investigated, and the infrared spectral characteristics from 1000 cm^{-1} to 4500 cm^{-1} of their plumes were measured. The experimental results indicate that the infrared radiation of the plume is influenced by the energy characteristics of the propellant.

(2) Radiative transfer calculation models for the propellant exhaust plumes were developed. By including the radiation source term in the energy equation, the plume field calculation and the radiative transfer calculation were carried out in a coupled way. The calculated results correspond with the experimental data, and the reliability of the models was verified.

(3) The modeling results show that the energy characteristics of the propellants have a great influence on the infrared radiation of the plume. The temperature distribution and the extent of the afterburning of the plume were different for the three propellants, and there is also great difference in the infrared radiation of the plume for the propellants.

(4) The influence of the radiation source term on the temperature of the plume flow field was studied. When the radiation energy emitted out of the fluid cell is larger than the received radiation energy from the circumambient fluid cells, the temperature of the fluid cell decreases with coupled solution.

Acknowledgment

This study was supported by the National Natural Science Foundation of China (Grant No. 11072032). The authors are very grateful to Wanxing Su, who gave many valuable suggestions on the writings of this paper.

References

1. Simmons FS. *Rocket exhaust plume phenomenology*. California: Aerospace Press; 2000.
2. Harwell KE, Jackson Jr HT, Poslajko F. Comparison of theoretical and experimental spatial distribution of infrared radiation in a rocket exhaust. AIAA-77-736; 1977.
3. Deimling L, Liehmann W, Eisenreich N, Weindeland M, Eckl W. Radiation emitted from rocket plumes. *Propellants Explos Pyrotech* 1997;**22**(3):152–5.
4. Devir AD, Lessin A, Cohen Y, Yaniv S, Kanelbaum Y, Avital G, et al. Comparison of calculated and measured radiation from a rocket motor plume. In: *39th AIAA aerospace sciences meeting & exhibit;* 2001 Jan 8-11; Nevada; 2001.
5. Nelson HF. Influence of particulates on infrared emission from tactical rocket exhausts. *J Spacecraft Rockets* 1984;**21**(5):425–32.
6. Nelson HF. Evaluation of rocket plume signature uncertainties. *J Spacecraft Rockets* 1987;**24**(6):546–51.
7. Freeman GN, Ludwig CB, Malkmus W, Reed R. Development and validation of standardized infrared radiation model (SIRRM). In: Edwards AFB, editor. Technical report. California: Air Force Rocket Propulsion Laboratory/Director of Science and Technology/Air Force Systems Command (US); 1979. Report No.: AFRPL-79-55.
8. Ludwig CB, Malkmus W. The standard infrared radiation model. In: *AIAA 16th thermophysics conference*; 1981 Jun 23-25; California; 1981.
9. Surzhikov ST. Spectral and narrow band directional emissivity of light-scattering and non-scattering volumes. In: *Eight AIAA/ASME joint thermophysics and heat conference*; 2002 Jun 24-26; St. Louis; 2002.
10. Surzhikov ST. Monte Carlo simulation of plumes spectral Emission. In: *36th AIAA thermophysics conference*; 2003 Jun 23-26; Orlando; 2003.
11. Surzhikov ST. Direct simulation Monte-Carlo algorithms for the rocket exhaust plumes emissivity prediction. In: *40th AIAA aerospace sciences meeting & exhibit*; 2002 Jan 14-17; Nevada; 2002.
12. Burt JM, Boyd ID. A Monte Carlo radiation model for simulating rarefied multiphase plume flows. In: *38th AIAA thermophysics conference*; 2005 Jun 6-9; Toronto; 2005.
13. Burt JM, Boyd ID. Monte Carlo simulation of particle radiation in high altitude solid rocket plumes. In: *43rd AIAA/ASME/SAE/ASEEJoint propulsion conference & exhibit*; 2007 Jul 8-11; Cincinnati; 2007.
14. Liu J, Shang HM, Chen YS, Wang TS. GRASP: a general radiation simulation program. In: *32nd thermophysics conference*; 1997 Jun 23-25; Atlanta; 1997.
15. Pergament HS, Jensen DE. Influence of chemical kinetic and turbulent transport coefficients on afterburning rocket plumes. *J Spacecraft Rockets* 1971;**8**(6):643–9.
16. Jensen DE, Jones GA. Reaction rate coefficients for flame calculations. *Combust Flame* 1978;**32**:1–34.
17. Avital G, Cohen Y, Gamss L, Kanelbaum Y, Macales J, Trieman B, et al. Experimental and computational study of infrared emission from underexpanded rocket exhaust plumes. *J Thermophys Heat Transfer* 2001;**15**(4):377–83.
18. Yakhot V, Orszag SA. Renormalization group analysis of turbulence: I. Basic theory. *J Sci Comput* 1986;**1**(1):3–51.
19. Brentner KS, Gimelshein SF, Levin DA. Investigation of soot combustion in under expanded Jet plume flows. In: *41st Aerospace sciences meeting and exhibit*; 2003 Jan 6-9; Nevada; 2003.
20. Modest MF. *Radiative heat transfer*. 2nd ed. San Diego: Academic Press; 2003.
21. Rothman LS, Jacquemart D, Barbe A, Bennerc DC, Birkd M, Browne LR, et al. The HITRAN 2004 molecular spectroscopic database. *J Quant Spectrosc Radiat Transfer* 2005;**96**(2):139–204.
22. Young SJ. Nonisothermal band model theory. *J Quant Spectrosc Radiat Transfer* 1977;**18**(1):1–28.

Wang Weichen is a Ph.D. candidate in Beijing Institute of Technology. His main research interest lies in the infrared radiation signature of exhaust plume from solid propellants.

Li Shipeng is an associate professor in Beijing Institute of Technology. His main research interest lies in engineering design of solid rocket motor.